Absorption of blue light by cigarette smoke components is highly toxic for retinal pigmented epithelial cells

Corinne Zinflou & Patrick J. Rochette

Archives of Toxicology

ISSN 0340-5761

Arch Toxicol
DOI 10.1007/s00204-018-2344-3

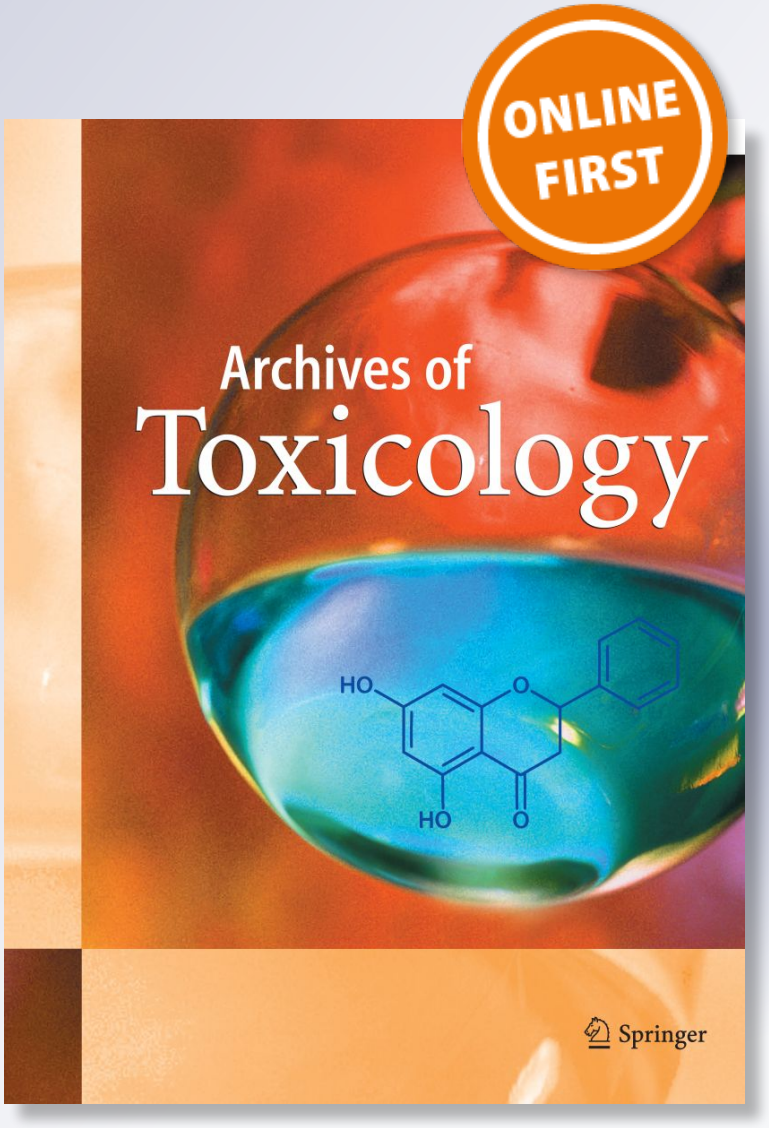

Springer

Archives of Toxicology
https://doi.org/10.1007/s00204-018-2344-3

ORGAN TOXICITY AND MECHANISMS

Absorption of blue light by cigarette smoke components is highly toxic for retinal pigmented epithelial cells

Corinne Zinflou[1,2] · **Patrick J. Rochette**[1,2,3]

Received: 20 July 2018 / Accepted: 5 November 2018

Abstract

Lesion to the retinal pigment epithelium (RPE) is a crucial event in the development of age-related macular degeneration (AMD), the leading cause of blindness in industrialized countries. Tobacco smoking and high-energy visible blue (HEV; 400–500 nm) light exposure are major environmental risk factors for AMD. Individually, they have been shown to cause damage to the RPE. Tobacco smoke contains toxic polycyclic aromatic hydrocarbons (PAH) that can accumulate in RPE and which absorb HEV light. It can thus be postulated that the interaction between both factors in RPE cells can have a synergic toxic effect to the RPE. To test this hypothesis, cultured human RPE cells (ARPE19) were treated with nanomolar concentrations of benzo[a]pyrene (BaP) or indeno[1,2,3-cd]pyrene (IcdP), then exposed to HEV light using an irradiation system that mimics the solar spectrum normally transmitted to the retina through the human ocular media. Using mitochondrial network morphology changes and key features of AMD-related RPE defects such as apoptotic cell death and oxidative stress, we demonstrate that a synergistic phototoxicity is generated when nanomolar concentrations (≤ 500 nM) of IcdP interact with sub-lethal amounts of HEV light. Indeed, we found IcdP to be at least 3000 times more toxic for RPE cells when irradiated with HEV light. This synergy translates into disruption of mitochondrial network, ROS enhanced accumulation and apoptosis of RPE cells. Our results underline an important interplay between two environmental risk factors involved in AMD progression and strongly indicate that IcdP, upon interaction with HEV light, may initiate the biological mechanisms underlying the association between cigarette smoking and AMD-related RPE degeneration.

Keywords Age-related macular degeneration · Polycyclic aromatic hydrocarbons · Benzo[a]pyrene · Indeno[1,2,3-cd]pyrene · High energy visible blue light · Oxidative stress

Introduction

Age-related macular degeneration (AMD) is the world's third largest cause of blindness and moderate–severe vision impairment (Bourne et al. 2013), and the leading cause of irreversible vision loss among adults aged 50 years and older in the Western world (Bourne et al. 2013; Wong et al. 2014). The lack of existing curative treatments for AMD (Ambati and Fowler 2012; Lim et al. 2012) has prompted research efforts to focus on understanding its etiology and identifying risk factors. AMD is a complex multifactorial disease, whose pathogenesis is thought to be associated with genetic predisposition, medical conditions and environmental risk factors. Aside from unmodifiable factors such as advanced age, gender and genetic polymorphisms (Bourne et al. 2013; Chakravarthy et al. 2010; Fritsche et al. 2014; Wong et al. 2014), epidemiological studies have identified several controllable factors with a significant impact on AMD progression. Some of these include smoking, poor dietary intake of antioxidants, diabetes, cardiovascular risk factors, high body mass index and sunlight exposure (Chakravarthy et al. 2010; Lambert et al. 2016; Sui et al. 2013; Thornton et al.

Electronic supplementary material The online version of this article (https://doi.org/10.1007/s00204-018-2344-3) contains supplementary material, which is available to authorized users.

✉ Patrick J. Rochette
Patrick.rochette@orlo.ulaval.ca

[1] Centre de Recherche du CHU de Québec-Université Laval, Axe Médecine Régénératrice, Hôpital du Saint-Sacrement, Québec, QC, Canada

[2] Centre de Recherche en Organogénèse Expérimentale de l'Université Laval/LOEX, Québec, QC, Canada

[3] Département d'Ophtalmologie et ORL-chirurgie cervico-faciale, Université Laval, Quebec, QC, Canada

Published online: 13 November 2018

2005). However, the biological mechanisms related to these factors and involved in AMD development are still unknown.

Recently, experimental studies have investigated the implication of some modifiable risk factors on AMD development (Andriessen et al. 2016; Espinosa-Heidmann et al. 2006; Rowan et al. 2017) using human cell culture or animal models. In this respect, light exposure- and cigarette smoke-induced changes in the retinal pigment epithelium (RPE) received particular attention (Fujihara et al. 2008; King et al. 2004; Patton et al. 2002; Sparrow et al. 2000; Wihlmark et al. 1997). The RPE is a mono-layered epithelium lining the posterior side of the retina. It is formed of highly specialized post-mitotic cells that maintain photoreceptors health and support their function in the visual cycle. Vision loss in AMD is ultimately caused by deterioration of the RPE and subsequent degeneration of photoreceptors (Ambati and Fowler 2012; Dunaief et al. 2002; Young 1987). The oxidative lesions associated with AMD development (Chiras et al. 2015; Ebrahimi et al. 2018; Hollyfield et al. 2008; Kaya et al. 2012; Rabin et al. 2013) and the protective effect of antioxidant supplementation against AMD progression [reviewed in (Schmidl et al. 2015)] have led to hypothesize that oxidative stress is a major contributor to AMD-related RPE defects.

Light exposure produces photochemical lesions to the RPE (Hafezi et al. 1997; Lerman 1980). Given the transmission properties of human ocular media (Boettner and Wolter 1962), blue radiations (400–500 nm) are the most energetic and potentially damaging wavelengths reaching adults' RPE cells (Sparrow et al. 2000). Blue light, also known as high energy visible (HEV) light, has been reported to impair RPE functionality (Putting et al. 1994). At high doses, HEV light induces RPE cells apoptosis (Sparrow et al. 2000), disrupts lysosome membranes and promotes the leakage of hydrolytic enzymes (Wihlmark et al. 1997). Photo-oxidative processes, mediated through the sensitization of lipofuscin components in aging RPE (Sparrow et al. 2000; Wielgus et al. 2010; Wihlmark et al. 1997) and/or mitochondrial chromophores (King et al. 2004), are suggested as a critical mechanism for HEV light-induced toxicity in RPE cells (King et al. 2004; Wihlmark et al. 1997).

Cigarette smoking is the modifiable risk factor the most consistently associated with AMD (Chakravarthy et al. 2010; Thornton et al. 2005). Experimental evidences indicate that tobacco smoke exposure triggers many AMD-like features in RPE, including histopathological damage (Espinosa-Heidmann et al. 2006; Fujihara et al. 2008), oxidative injury (Bertram et al. 2009), alteration of extracellular matrix or inflammatory gene expression (Bertram et al. 2009; Espinosa-Heidmann et al. 2006) and apoptosis (Bertram et al. 2009; Fujihara et al. 2008). Polycyclic aromatic hydrocarbons (PAH) byproducts, generated by the incomplete combustion of organic matters, represent one of the most toxic compounds found in cigarette smoke. High-molecular weight PAH, such as the benzo[a]pyrene (BaP), have been shown to exert a cytotoxic effect on cultured RPE cells when they were exposed to extracellular concentrations equal or greater than 50 µM (Patton et al. 2002; Sharma et al. 2008; Wang et al. 2009). In addition, exposures to sub-lethal PAH concentrations (10 µM) have been associated with RPE lysosomal and exocytotic activities alterations (Wang et al. 2009).

PAH are carried through the bloodstream and distributed throughout the body to different locations including ocular tissues (Roberto et al. 1996). There, they are retained and concentrated in melanin-rich tissues, such as the RPE (Roberto et al. 1996). Owing to the arrangement of benzene rings in their structure, PAH usually absorb light photons in the ultraviolet (UV) range and increased toxicities associated with UV absorption by some PAH are well documented (Burke and Wei 2009; Schirmer et al. 1998; Soeur et al. 2017; Wang et al. 2007). A few PAH with four or more fused rings may also absorb HEV light photons. Therefore, an interaction between PAH accumulated in RPE cells and exposure to HEV radiations could exacerbate the stress caused by either factor alone. This study thus aimed to assess the toxic effects of PAH and HEV light combination in RPE cells. Using an irradiation system that mimics the solar spectrum normally transmitted to the retina through the human ocular media, we investigated the combined effects of nanomolar concentrations ($\leq$ 500 nM) of tobacco-derived PAH and sub-lethal HEV light doses on cultured human RPE cells (ARPE19). We used established AMD-related changes such as RPE cell death and oxidative stress as indicators of toxicity. Since mitochondria network is remodeled in response to toxic conditions (Karbowski and Youle 2003), we also examined whether RPE mitochondrial network was affected by PAH and HEV light combination. Our results highlight, for the first time to our knowledge, a strong and toxic synergistic interaction between the indeno[1,2,3-cd] pyrene (IcdP) and HEV light in RPE cells. We found that, associated with IcdP in concentrations lower than 500 nM, normally sub-lethal HEV light doses become highly cytotoxic in RPE. Our study underlines the interplay of modifiable risk factors involved in AMD onset and/or progression. This is particularly relevant for smokers, since such a synergy between HEV light and IcdP may contribute to their greater risk of developing AMD.

Materials and methods

All experiments performed in this study were conducted in accordance with our institution's guidelines and the Declaration of Helsinki.

Cell culture

The spontaneously immortalized human RPE cell line ARPE19 (ATCC® CRL-2302™) was cultured to confluence in Dulbecco's modified Eagle's Medium (DMEM) (Corning cellgro, VA, USA), supplemented with 10% fetal bovine serum (Wisent, QC, CA) and penicillin/streptomycin (200 UI/ml penicillin and 200 µg/ml streptomycin; Wisent, QC, CA) at 37 °C, 5% CO_2. All experiments were performed on confluent monolayers of ARPE19 cells.

Light source and dosimetry

The light source consisted of an Oriel 1.6 kW solar simulator (SSL), with an ozone-free xenon short arc lamp combined to an air mass 1.5G filter (Newport, CA, USA). A yellow Schott long pass optical filter (GG420; Schott, PA, USA) was added to the system. The GG420 filter displays light filtration properties similar to that observed for the human ocular media (Boettner and Wolter 1962) (Fig. 1a) and was used to mimic the UV–visible radiation spectrum normally transmitted to the retina. The incident spectrum transmitted to ARPE19 cells through this configuration is depicted in Fig. 1b.

The total output of the SSL through the GG420 optical filter was measured prior to each irradiation session using a 1918-R Optical Power Meter (with a 818P high-power thermopile detector; Newport, CA, USA), and the fraction of the output in the HEV light range (400–500 nm) was determined according to the manufacturer instructions. HEV irradiance at cell surface was approximately 220 W/m^2.

PAH UV–visible absorbance spectra

All studied PAH (Sigma–Aldrich, ON, CA) were dissolved in dimethyl sulfoxide (DMSO). Absorbance spectra of the chemicals were recorded over the 250–1100 nm range using a scanning UV–visible spectrophotometer (Varian Cary® 50 Bio UV–visible spectrophotometer), after a baseline correction made with DMSO.

PAH treatment and irradiation procedure

Confluent ARPE19 cells were incubated with the indicated concentrations of benzo[a]pyrene (BaP), indeno[1,2,3-cd]pyrene (IcdP) or vehicle (DMSO) in PBS for 30 min at 37 °C in the dark. They were then exposed to 100, 160, 220 or 320 J/cm^2 of HEV light in a cooling box using the SSL/GG420 setup (for irradiation periods of ~ 70, 120, 170 and 240 min, respectively). Unirradiated samples were kept in the dark at 4 °C for the length of corresponding irradiation. Immediately after the irradiation, PAH or vehicle solutions were removed. Cells were washed with PBS and allowed to recover in complete DMEM at 37 °C until analyses.

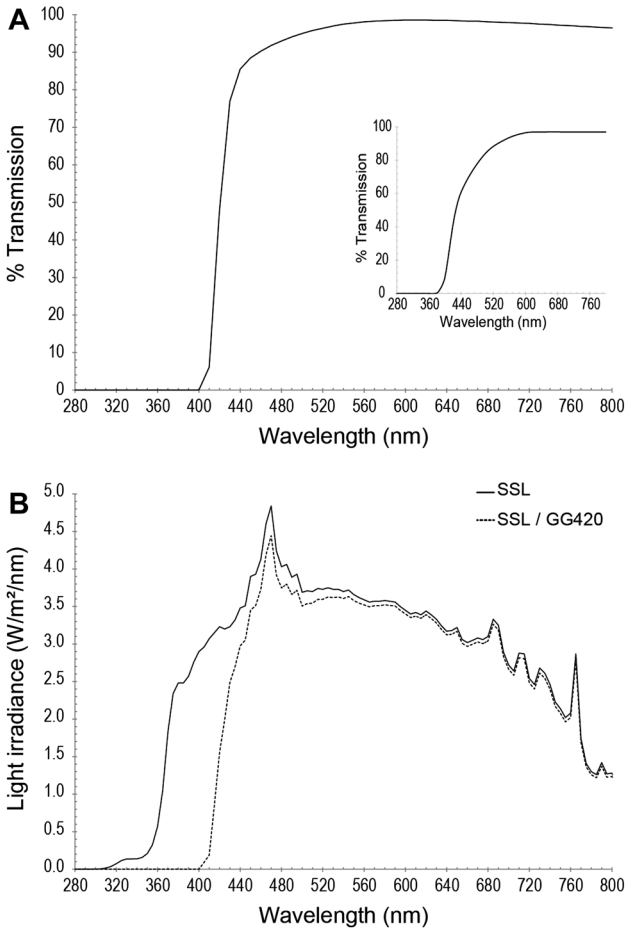

Fig. 1 Spectral characteristics of the SSL / GG420 filter setup. Light source consists of an Oriel solar simulator (SSL) with an ozone-free xenon short arc 1.6 kW lamp combined to an air mass 1.5G (AM1.5G) filter and a Schott GG420 long-pass optical filter. **a** Optical transmission of the Schott GG420 filter. The spectrum is derived from manufacturer's specifications. Insert shows the percent of light transmission through human ocular media [replotted from Boettner and Wolter (1962)]. **b** Spectral output produced by the SSL with the AM1.5G filter (solid line) and by the SSL equipped with the AM1.5G and the Schott GG420 filters (dashed line)

Antioxidant treatments

Cells were incubated with 5 mM of *N*-acetylcysteine (NAC; Sigma-Aldrich, ON, CA) or 10 µM of α-tocopherol (vitamin E; Sigma-Aldrich, ON, CA) in complete DMEM for 18–24 h prior to PAH treatment and/or HEV exposure. These agents were added back to the PAH or vehicle solutions during exposure and to the post-exposure medium.

Cytotoxicity assessment

Cytotoxicity of PAH and/or HEV exposure (in presence or absence of antioxidants) was assessed 24 h post-exposure using a MTS cell viability assay (CellTiter 96® AQueous Non-Radioactive Cell Proliferation Assay; Promega, WI, USA), according to the manufacturer protocol to measure viable cell metabolism. Optical density values were read at 490 nm using a microplate reader (BioRad 550 Microplate Reader). After correcting for background absorbance, the average absorbance of specified control was used as a baseline metabolic activity (value 1). Each experimental condition was assayed in independent quadruplicate.

Mitochondrial fluorescent staining

Consequences of PAH treatments and/or HEV exposure on mitochondrial network organization were assessed 1 h and 24 h after the irradiation, by fluorescent staining of mitochondria, using chloromethyl-X-rosamine (CMXRos Mito-Tracker Red; Invitrogen) labeling (Poot et al. 1996). The CMXRos dye is a cationic and mitochondrion-specific probe, relying on mitochondrial transmembrane potential to accumulate in mitochondria. For IcdP-treated cells, at the indicated period after the irradiation, cells were incubated in a staining medium containing 100 nM of CMXRos and 2 µg/ml of diamidino-2-phenylindole (DAPI; ThermoFisher, ON, CA) in complete DMEM for 15 min at 37 °C. Imaging was performed using a Zeiss Axioimager Z2 microscope equipped with appropriate filter sets and coupled with a Zeiss AxioCam MRm Rev 3 Monochromatic Digital Camera.

BaP displays a strong intrinsic fluorescence when excited by UV radiations (~ 365 nm). Its emission spectrum has been shown to peak at 405 and 430 nm (Rivera-Figueroa et al. 2004), preventing the use of DAPI as nuclear counterstain. Therefore, BaP-treated cells were stained with 100 nM of CMXRos in complete DMEM for 15 min at 37 °C. They were then placed in a solution of 10 µM of DRAQ5™ (Abcam, ON, CA) in complete DMEM (for nuclear staining) for 5 min at 37 °C. Labeled cells were imaged as described above. In parallel, based on the fluorescent properties of the BaP, images of BaP fluorescent emissions were also captured 1 and 24 h following the end of irradiation. Each experimental condition was tested at least in independent duplicate.

Cell death analysis

PAH treatments and/or HEV exposure-induced cell death was analyzed by flow cytometry using the FITC Annexin-V/Dead Cell Apoptosis kit (Invitrogen, OR, USA) according to the manufacturer protocol. Briefly, 16 h after the exposure to PAH and/or HEV light, ARPE19 cells were harvested and resuspended in Annexin-V buffer at a density of 1.5×10^6 cells/ml. Cells were mixed with 5% (v/v) of FITC Annexin-V and 1 µg/ml of propidium iodide (PI), then incubated at room temperature for 15 min. Analysis of apoptotic (Annexin-V positive cells) and necrotic/dead cells (PI positive cells) was performed with a BD Accuri C6 flow cytometer (BD Biosciences, ON, CA). Each experimental condition was assayed at least in independent triplicate.

ROS content analysis

Intracellular ROS content was measured using the oxidant-sensitive fluorescent probe chloromethyl-2′,7′-dichlorodihydrofluorescein diacetate, acetyl ester (CM-H_2DCFDA; Thermo-Fisher, ON, CA) and assayed as previously described (Wang and Joseph 1999) with minor modifications. Briefly, PAH- or vehicle-treated ARPE19 cells were exposed to HEV light as described above (with or without specified antioxidant pretreatment). Immediately at the end of irradiation, cells were incubated with 5 µM CM-H_2DCFDA in PBS (with or without added antioxidant) for 30 min at 37 °C. CM-H_2DCFDA was replaced by PBS (with or without added antioxidant) and the cells were incubated for a further 30 min at 37 °C. The fluorescence of cells in each well was recorded (0, 30 and 60 min following CM-H_2DCFDA addition) using a CytoFluor® Series 4000 multi-well fluorescence plate reader (Applied Biosystems, MA, USA) with excitation and emission filters set at 480 ± 10 and 530 ± 12.5 nm, respectively. For each well, a percentage increase in intracellular levels of ROS was determined at $t = 60$ min as a function of the percentage increase in CM-H_2DCFDA fluorescence calculated as described by (Wang and Joseph 1999). Each condition was tested in 4 independent replicates.

Statistical analysis

Data are presented as mean ± SD (standard deviation) of independent experiments. Statistical analysis was performed using KaleidaGraph software (Synergy Software, PA, USA). Differences between groups were assessed with the two-tailed homoscedastic student's t test or with one-way analysis of variance (ANOVA) followed by Dunnett or Tukey HSD procedures as post hoc tests. Significance level was defined for p value ≤ 0.05.

Results

Synergistic cytotoxicity induced by IcdP and HEV light

We measured the UV–visible absorbance spectra of 15 major PAH, which levels and distribution profiles in cigarette smoke have been previously investigated (Ding et al. 2005, 2006; Hoffmann et al. 2001; Lodovici et al. 2004; Vu et al. 2015) (Fig. 2 and S1). Among them, 3 possess HEV light (400–500 nm) absorption capacity: benzo[k]fluoranthene (BkF), benzo[a]pyrene (BaP) and indeno[1,2,3-cd] pyrene (IcdP). Toxic interactions between these and HEV light can, therefore, be anticipated. Both BkF and BaP compounds have relatively small HEV absorption bands with maxima at 404.5 and 405.5 nm, respectively (Fig. S1L and 2A). On the other hand, IcdP spectrum is characterized by a broad HEV absorption band with a maximum at 408.0 nm and shoulders between 420 and 485 nm (Fig. 2b).

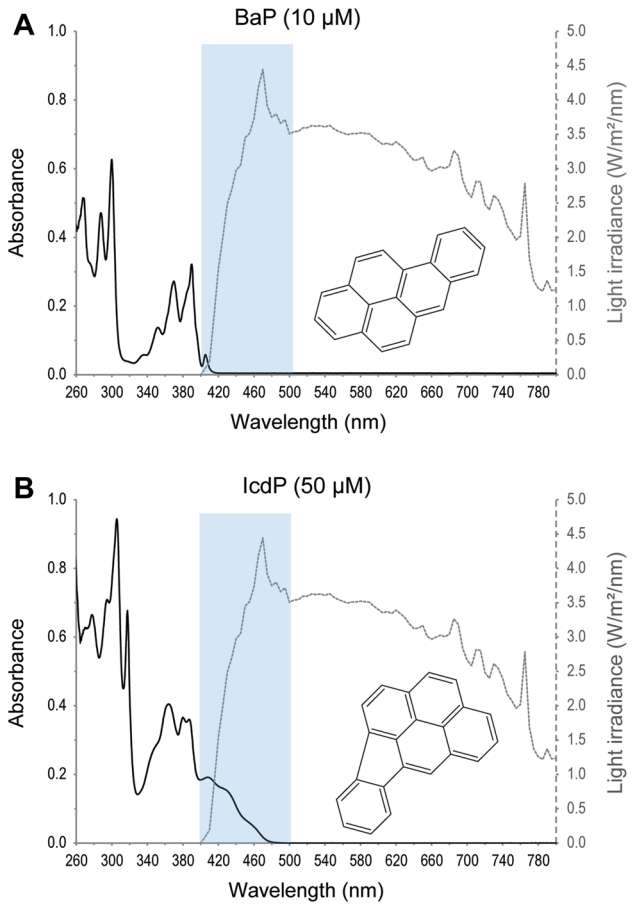

Fig. 2 BaP and IcdP light absorption spectra. Absorption spectra (solid lines) between 260 and 800 nm were obtained using a scanning Varian Cary® 50 Bio UV–visible spectrophotometer for **a** 10 µM benzo(a)pyrene (BaP) or **b** 50 µM indeno[1,2,3-cd]pyrene (IcdP) dissolved in DMSO. The chemical structure of each compound is depicted. Absorption spectra are overlaid with the emission spectrum produced by the SSL/GG420 setup (dashed gray line) and the HEV light range (400–500 nm) is indicated by the shaded blue area. (Color figure online)

Potential toxic interactions between HEV-absorbing PAH and the HEV radiations normally reaching adult human eye fundus were evaluated for IcdP and BaP, using cell viability as an indicator of toxicity. ARPE19 cells, treated with different concentrations of IcdP (15–500 nM) or BaP (2.5 to 200 nM), were exposed to HEV light (100, 160, 220 or 320 J/cm^2). ARPE19 cell viability, reflected by their mitochondrial activity, was measured 24 h post-exposure (Fig. 3a, d). Exposure to HEV light alone induces no loss of ARPE19 cell viability (Fig. 3a). On the contrary, compared to unirradiated cells activity level, exposure to 320 J/cm^2 HEV induces a twofold increased mitochondrial activity. Likewise, we observed that neither IcdP (up to 1 µM) nor BaP (up to 200 nM) treatments alone lead to significant change in ARPE19 cells viability (Fig. S2–S3). However, combination of HEV light and IcdP, in a concentration of 75 nM or greater, induces a dose-dependent loss of cell viability (Fig. 3a). For cells treated with 75 nM IcdP, HEV light toxicity becomes apparent only for the highest tested dose (320 J/cm^2), where mitochondrial activity is reduced to 16% of the activity in unirradiated cells. When combined with 150 nM IcdP treatment, exposure to HEV light reduces ARPE19 cells activity to 56% of unirradiated cells level at 220 J/cm^2 (although it did not reach significance; $p = 0.054$), and to background level at 320 J/cm^2. In 250 and 500 nM IcdP-treated cells, we noted that HEV light readily induces a significant decrease in cell viability from 160 J/cm^2. Indeed, after a 160 J/cm^2 HEV light exposure, ARPE19 cell activity drops to 61 and 23%, for cells treated with 250 and 500 nM IcdP, respectively (Fig. 3a). Combination of HEV light and BaP (up to 200 nM) does not reduce ARPE19 cells viability below unirradiated cells level (Fig. 3d). Nonetheless, the HEV-induced enhancement of cell metabolism observed at 320 J/cm^2 is not observable in BaP-treated cells, indicating that mitochondrial activity is relatively reduced. Taken together, our data indicate that nanomolar concentrations of IcdP and HEV radiations reaching human eye fundus have synergetic toxic effects on ARPE19 cells.

IcdP and HEV light interaction results in mitochondrial network disruption

Toxic interactions between HEV light and PAH were further investigated using changes in mitochondrial network morphology. Mitochondrial network visualization was achieved by CMXRos fluorescent staining of mitochondria in ARPE19 cells, 1 h and 24 h following exposure to PAH and/or HEV (160 J/cm^2) (Fig. 3b, c, e). In ARPE19 cells exposed or not to HEV light alone, mitochondria form a complex

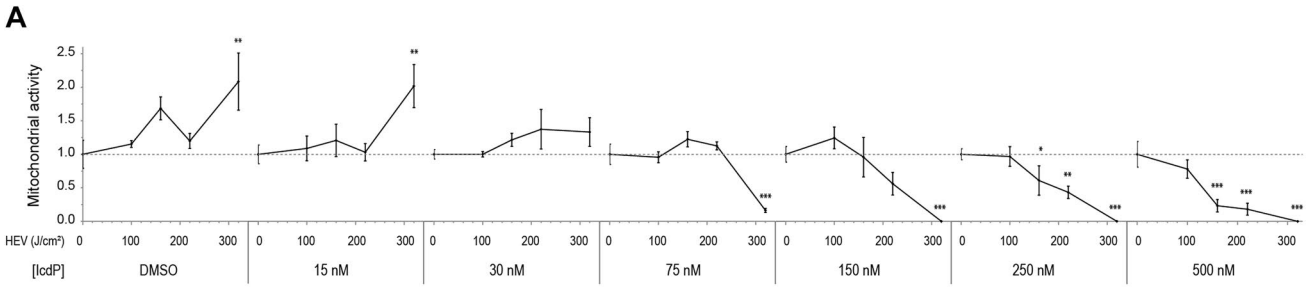

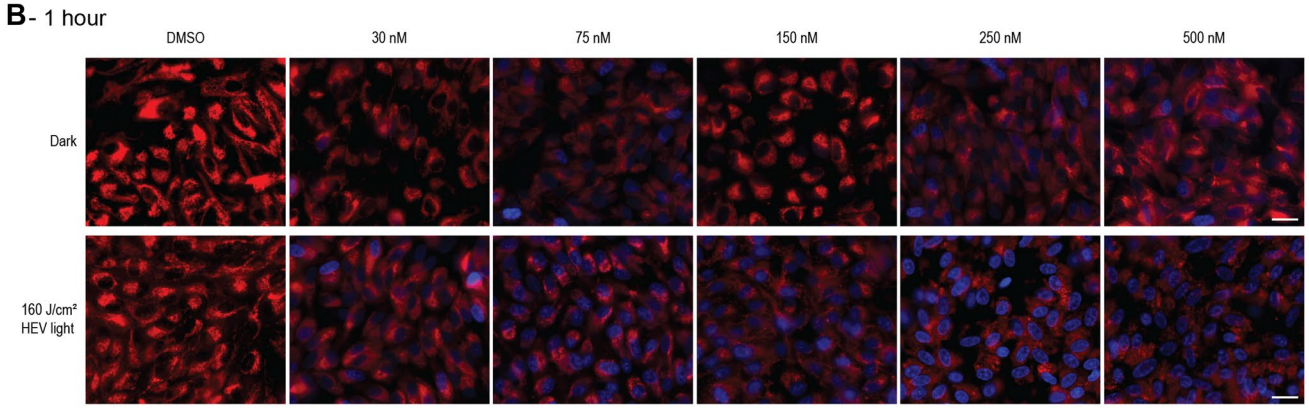

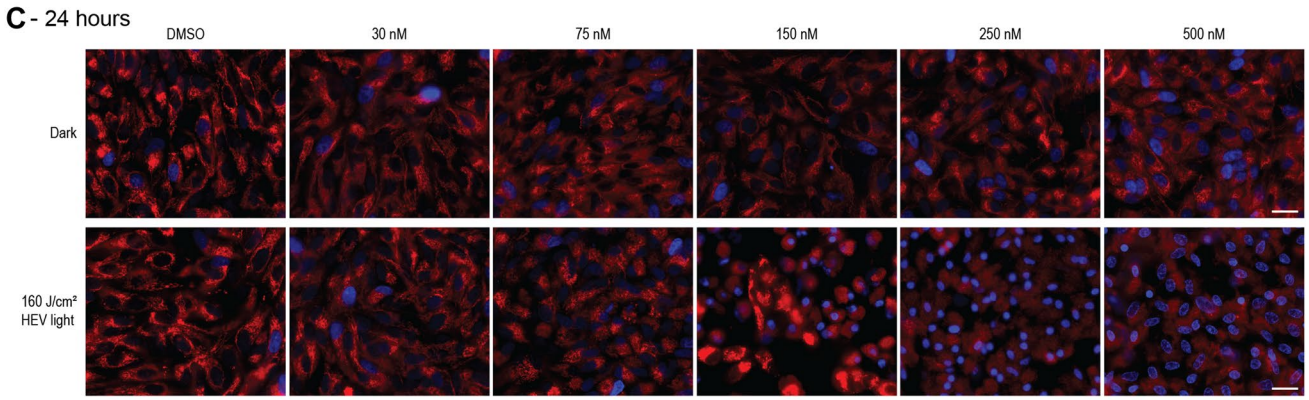

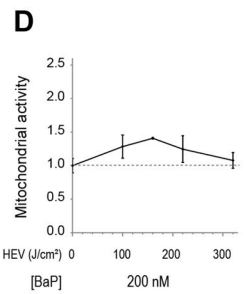

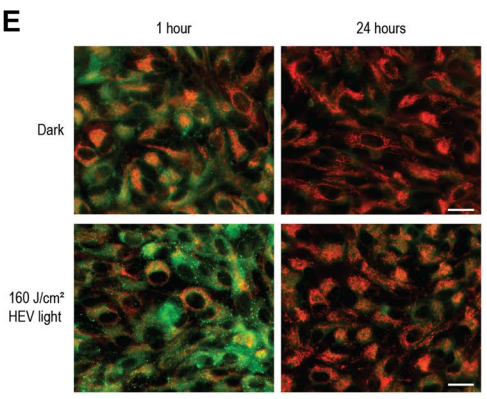

◂**Fig. 3** Toxicity and consequences on metabolic activity produced by co-exposure to IcdP and HEV light. **a** ARPE19 cells treated with vehicle (DMSO) or increasing concentrations of IcdP (15–500 nM) were kept in the dark or exposed to HEV light (100, 160, 220 or 320 J/cm^2). Mitochondrial activity was measured 24 h later using the MTS assay to estimate cell viability. For each IcdP concentration, unirradiated cells activity was used as the baseline (value 1) and a relative cell activity was obtained for each HEV light amount. **b, c** Representative images of mitochondrial network staining in ARPE19 cells, 1 h (**b**) and 24 h (**c**) after exposure to IcdP (0–500 nM) in the dark (upper panels) or combined with a 160 J/cm^2 HEV light exposure (lower panels). Mitochondria were revealed using CMXRos dye (red) and DAPI counterstain (blue) was used to assess nuclei characteristics. **d** Relative viability of ARPE19 cells measured 24 h after treatment with 200 nM BaP in the dark or exposed to increasing amounts of HEV light (100, 160, 220 or 320 J/cm^2). Unirradiated cells activity was used as the baseline (value 1). **e** Representative images of mitochondrial network staining in ARPE19, 1 h and 24 h after exposure to 200 nM BaP without (upper panels) or with a 160 J/cm^2 HEV light exposure (lower panels). Along with mitochondria (red) organization, BaP intrinsic fluorescence imaging (green) reveals time-dependent distribution of BaP in ARPE19 cells. Error bars are standard deviation (SD) from 4 independent experiments (**a, d**). *$p < 0.05$, **$p < 0.01$ and ***$p < 0.001$ versus unirradiated control [one-way analysis of variance (ANOVA) with Dunnett procedure as post hoc test]. Scale bar = 20 µm (**b, c** and **e**). (Color figure online)

network of elongated tubules oriented in a few dominant directions (Fig. 3b, c); characteristic of healthy functional mitochondria. In addition, in our experimental conditions, cells are poorly permeant to nuclear counterstains. The same features are noted in 200 nM BaP-treated cells with or without HEV irradiation (Fig. 3e). It is noteworthy that fluorescent detection of BaP confirms the cellular uptake and cytoplasmic internalization of PAH by ARPE19 cells. The loss of fluorescence after 24 h also indicates their processing and elimination by ARPE19 cells.

In response to IcdP treatments (30–500 nM) alone, mitochondria retain a tubular shape, though their arrangement and orientation seem much less clearly defined with increasing IcdP concentrations after 1 h (Fig. 3b—upper panels). However, these are restored after 24 h (Fig. 3c—upper panels). Exposure of IcdP-treated cells to 160 J/cm^2 HEV light is associated with an increased permeability of ARPE19 cells for the nuclear dye, 1 h after exposure (Fig. 3b—lower panels), along with different changes in mitochondrial network morphology, including network fragmentation and mitochondria clustering. Moreover, mitochondria tubular shape and organization are disrupted in a IcdP concentration-dependent manner with a complete loss of the network and scattered spherical mitochondria observed with the highest tested IcdP concentration (Fig. 3b—lower panels).

A complete to almost complete restoration of mitochondrial network can be observed after 24 h in 30 nM IcdP/HEV- and 75 nM IcdP/HEV- exposed cells (Fig. 3c—lower panels). 24 h after exposure, 150, 250 and 500 nM IcdP/HEV-exposed cells display disintegrated mitochondrial networks (with only a few cells showing a partially restored network after 150 nM IcdP/HEV exposure). Besides, nuclei mainly appear shrunken, fragmented (in 150 nM IcdP/HEV-exposed cells) or with unevenly condensed DNA content (in 500 nM IcdP/HEV-exposed cells). Taken together, these results confirm the synergistic toxicity resulting from HEV light and IcdP interaction in ARPE19 cells. They indicate that co-exposure of ARPE19 cells to nanomolar concentrations of IcdP and HEV light can quickly lead to major and irreversible disruptions of mitochondrial network integrity.

Synergistic induction of apoptosis by IcdP and HEV light

To assess the consequences of IcdP and HEV light synergistic toxicity, ARPE19 cell death (apoptosis and necrosis) following PAH and/or HEV light exposure was determined (Fig. 4). ARPE19 cells, treated with IcdP (250 nM), BaP (250 nM) or vehicle (DMSO), were exposed to increasing amounts of HEV light (100–320 J/cm^2). Unirradiated PAH- or DMSO-treated cells were kept in the dark for the duration of exposures. Neither IcdP (Fig. 4a–d) nor BaP (Fig. 4e, f) treatments alone affect ARPE19 cells survival. Likewise, exposure to HEV light alone (up to 320 J/cm^2) induces no significant cell death. In contrast, in ARPE19 cells treated with IcdP, HEV light triggers a significant level of cell death by apoptosis in a dose-dependent manner (Fig. 4a–d). Indeed, the average level of apoptotic cells is 7.6, 21.7, 43.8 and 67.7% in IcdP-treated cells exposed to 100, 160, 220 and 320 J/cm^2 of HEV light, respectively. Although not significant, a higher level of necrosis can be observed in IcdP-treated cells exposed to 100 J/cm^2 of HEV light (Fig. 4a).

Irradiation of BaP-treated ARPE19 cells with up to 220 J/cm^2 of HEV light does not significantly induce cell death (Fig. 4e). However, a significant increase in necrosis (4.0%) and apoptosis (17.1%) was found at the highest HEV dose used (320 J/cm^2) in BaP-exposed ARPE19 (Fig. 4f). Our results indicate that IcdP and HEV light interaction triggers apoptotic events in ARPE19 cells.

Synergistic induction of oxidative stress by IcdP and HEV light

ROS accumulation in ARPE19 cells treated with vehicle (DMSO), BaP (200 nM) or IcdP (15–500 nM) and/or exposed to HEV light (160 J/cm^2) was determined 60 min after the exposure using the oxidant-sensitive indicator CM-H_2DCFDA (Fig. 5). BaP or IcdP treatments alone do not affect ROS accumulation. In addition, exposure to 160 J/cm^2 HEV light alone or in combination with 200 nM BaP induces no significant variations in ROS accumulation.

However, in ARPE19 cells treated with IcdP concentrations equal or higher than 30 nM, HEV light irradiation leads to a

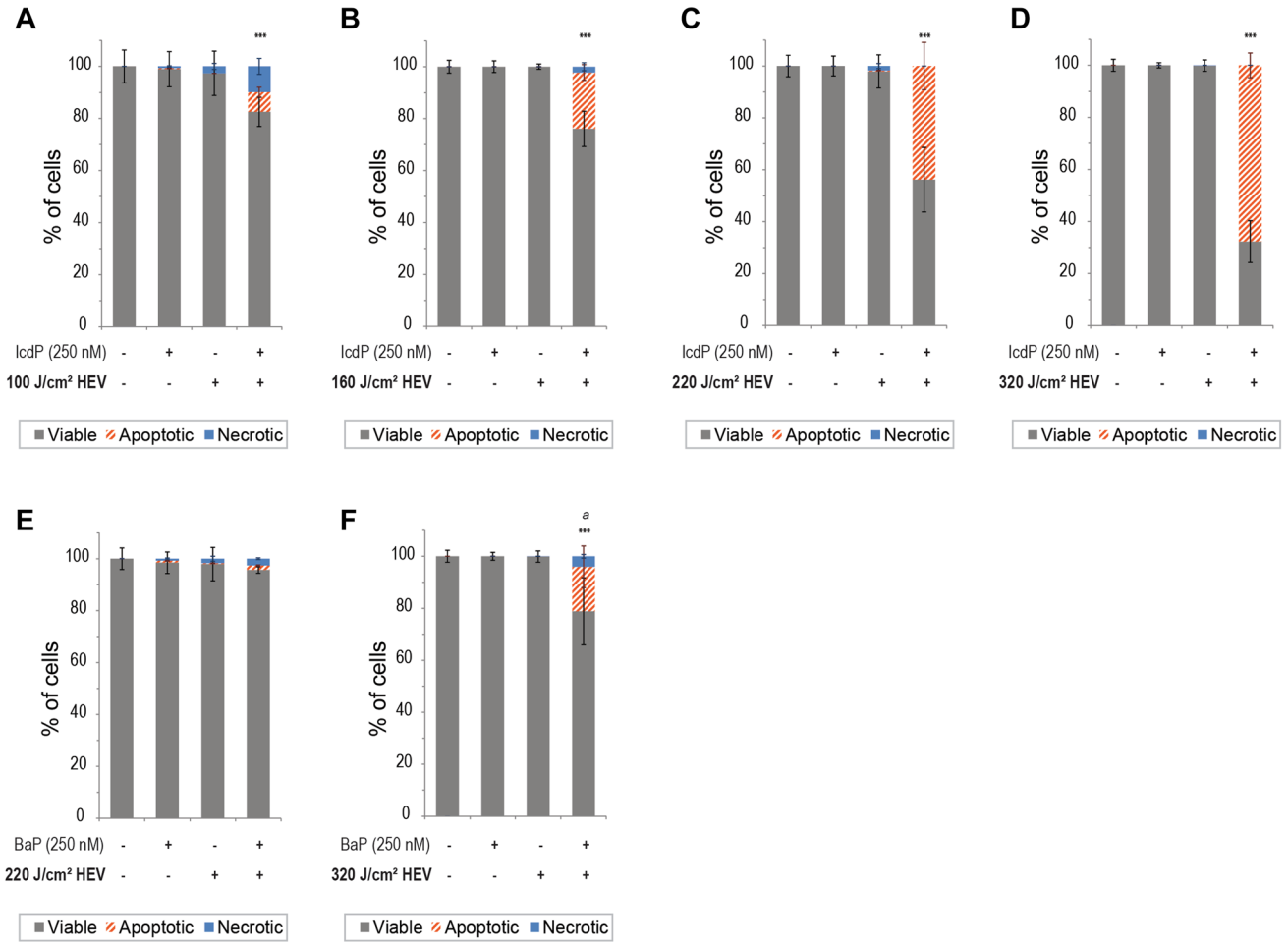

Fig. 4 Synergistic induction of apoptosis by IcdP and HEV light. ARPE19 cells were treated with 250 nM IcdP (**a**–**d**) or 250 nM BaP (**e**–**f**), then kept in the dark or exposed to 100 J/cm^2 (**a**), 160 J/cm^2 (**b**), 220 J/cm^2 (**c, e**) or 320 J/cm^2 (**d, f**) of HEV light. Viable (grey bars), apoptotic (dashed orange bars) and necrotic/dead (blue bars) cells levels were analyzed by flow cytometry using Annexin V/PI double staining. Error bars are sd from at least 3 independent experiments. (*) are for differences in apoptotic cells levels versus controls and (^{a}) are for differences in necrotic cells levels *versus* controls. $^a p < 0.05$ and $^{***}p < 0.001$ [one-way analysis of variance (ANOVA) with Tukey HSD procedure as post hoc test]. (Color figure online)

significant acceleration of ROS accumulation (Fig. 5). Indeed, for cells treated with 30 or 75 nM IcdP, intracellular ROS accumulation is 1.2 time faster in HEV-exposed cells than in unirradiated cells. More pronounced HEV light-induced enhancements of ROS accumulation rate are noted with higher IcdP concentrations. ROS accumulation is 1.3, 1.7 and 2.8 times faster in HEV-exposed cells than in unirradiated cells, in presence of 150, 250 and 500 nM IcdP, respectively (Fig. 5). Our data show that HEV light and IcdP interaction rapidly promotes oxidative stress within ARPE19 cells.

Prevention of ROS accumulation improves IcdP/HEV-exposed ARPE19 cell viability

To assess the potential implication of oxidative stress in IcdP/HEV-induced ARPE19 cell death, we determined the effect of two broad spectrum ROS scavengers [α-tocopherol and *N*-Acetylcysteine (NAC)]. ARPE19 cells, incubated with 10 µM α-tocopherol or 5 mM NAC, were exposed to IcdP (150–500 nM) and/or HEV light (160 J/cm^2). ROS accumulation was monitored for 60 min after exposure and cell viability was assessed 24 h post-exposure. Figure 6 illustrates the effect of α-tocopherol (Fig. 6a) and NAC (Fig. 6b) incubation on ROS accumulation (upper panels) and cell viability (lower panels).

α-tocopherol efficiently reduces IcdP/HEV-induced ROS accumulation in ARPE19 cells (Fig. 6a, upper panel). Indeed, intracellular levels of ROS in IcdP/HEV-exposed cells increase in average by 10.0, 15.3 and 15.5% with 150, 250 and 500 nM IcdP treatments, respectively. In presence of α-tocopherol, ROS accumulation is significantly reduced to 6.7, 8.1 and 10.0% in HEV-exposed

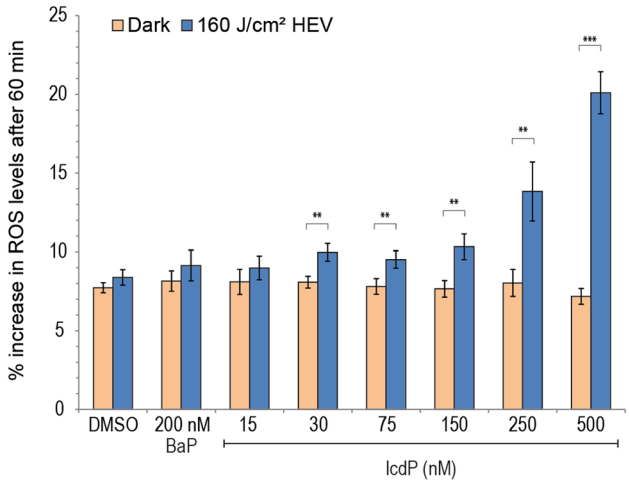

Fig. 5 ROS accumulation rate following IcdP plus HEV light co-exposure. ARPE19 cells treated with vehicle (DMSO), with 200 nM BaP or with increasing concentrations of IcdP (15–500 nM) were kept in the dark (orange bars) or exposed to 160 J/cm^2 HEV light (blue bars). General ROS accumulation was assessed using the oxidant-sensitive probe CM-H_2DCFDA, 60 min after the end of exposure. Error bars are sd from 4 independent experiments. $^{**}p < 0.01$ and $^{***}p < 0.001$ [two-tailed homoscedastic student's *t* test]. (Color figure online)

cells treated with 150, 250 and 500 nM IcdP, respectively. Moreover, α-tocopherol reduces the level of ROS in HEV-exposed cells treated with 150 or 250 nM IcdP to level similar to that of cells exposed to HEV light alone. The decrease in ROS buildup in IcdP/HEV-exposed cells associated with the presence of α-tocopherol is accompanied by improved ARPE19 cell viability 24 h post-exposure (Fig. 6a, lower panel). More precisely, α-tocopherol abolishes the loss of viability induced by IcdP and HEV light co-exposure when cells were treated with 150 or 250 nM IcdP, and prevents in average 65% of the loss induced by co-exposure to 500 nM IcdP and HEV light.

NAC is also efficient in reducing IcdP/HEV-induced ROS accumulation in ARPE19 cells at all tested IcdP concentrations (Fig. 6b, upper panel). NAC incubation significantly reduces average ROS increase in IcdP/HEV-exposed cells from 9.1, 12.3 and 15.5% to 6.8, 8.4 and 9.7%, when cells were treated with 150, 250 and 500 nM IcdP, respectively. However, NAC prevents the loss of ARPE19 cell viability only at the lowest tested IcdP concentration (Fig. 6b, lower panel). When cells were treated with 250 or 500 nM IcdP, we found no significant improvement of ARPE19 cell viability associated with NAC-induced decrease in ROS buildup in IcdP/HEV-exposed cells. Taken together, our results suggest that specific prevention of IcdP/HEV-induced ROS accumulation is associated with enhanced survival of ARPE19 cells exposed to both agents.

Discussion

The interactions between light and PAH has gained interest in recent years, with regards to skin disorders (Botta et al. 2009; Burke and Wei 2009; Marrot 2017; Mauthe et al. 1995; Soeur et al. 2017). In the eye, while HEV light and PAH have been evaluated independently for toxicity in RPE cells in regard to AMD development, their combined action has not been addressed. We thus aim to determine whether possible toxic interactions between HEV light and tobacco smoke-derived PAH exposures could take place in RPE cells and be involved in AMD-related RPE defects.

We used confluent monolayers of ARPE19 cells as a model of RPE and exposed them to non-lethal nanomolar concentrations of PAH to simulate a contamination of RPE by tobacco smoke-derived PAH. We focused on IcdP since it efficiently absorbs HEV wavelengths (Fig. 2). BaP, the most studied PAH, is often used as a surrogate for other PAH. It is considered as one of the most toxic PAH (Dabestani and Ivanov 1999). BaP does not significantly absorb HEV wavelengths (Fig. 2) and was then included in this study as a negative control of PAH/HEV interaction. In all experiments, ARPE19 cell monolayers were exposed to a visible light spectrum comparable to the one transmitted to adult human eye fundus through the ocular media (Fig. 1). To exclude the possibility that unfiltered UVA light from our light source could account for the observed results, BaP (2.5–200 nM) and IcdP (15–1000 nM) treated ARPE19 cells were exposed to 5 J/cm^2 UVA light along with 60 J/cm^2 HEV light, and then tested for cell viability 24 h later (supplementary methods). When UVA radiations are present, BaP is far more potent than IcdP in reducing ARPE19 cell viability (Fig. S2). Combined with UVA exposure, 50 nM BaP decreases cell activity to 36% of unirradiated cell activity (Fig. S2C), whereas in IcdP-treated cells, such reduction is achieved with a concentration of 250 nM (Fig. S2D).

One important finding from this research is that a synergistic phototoxic effect is generated within RPE cells by the interaction between internalized IcdP and the HEV light radiations normally reaching the retina. We revealed that exposure to IcdP concentrations of 500 nM or less, significantly and dose-dependently lowers the threshold dose for HEV light cytotoxicity in RPE cells, even when no or very limited toxicity is produced by either factor alone. In fact, we found that an association of HEV light with concentrations of IcdP as low as 150 nM is enough to exert toxic and metabolic effects that compromise RPE cells survival (Fig. 3). However, no toxic effect is observed in RPE cells after treatments with pre-irradiated IcdP (Fig. S3-A) or after sequential exposure to HEV first then to IcdP (Fig.S3-B). Both HEV light and IcdP need

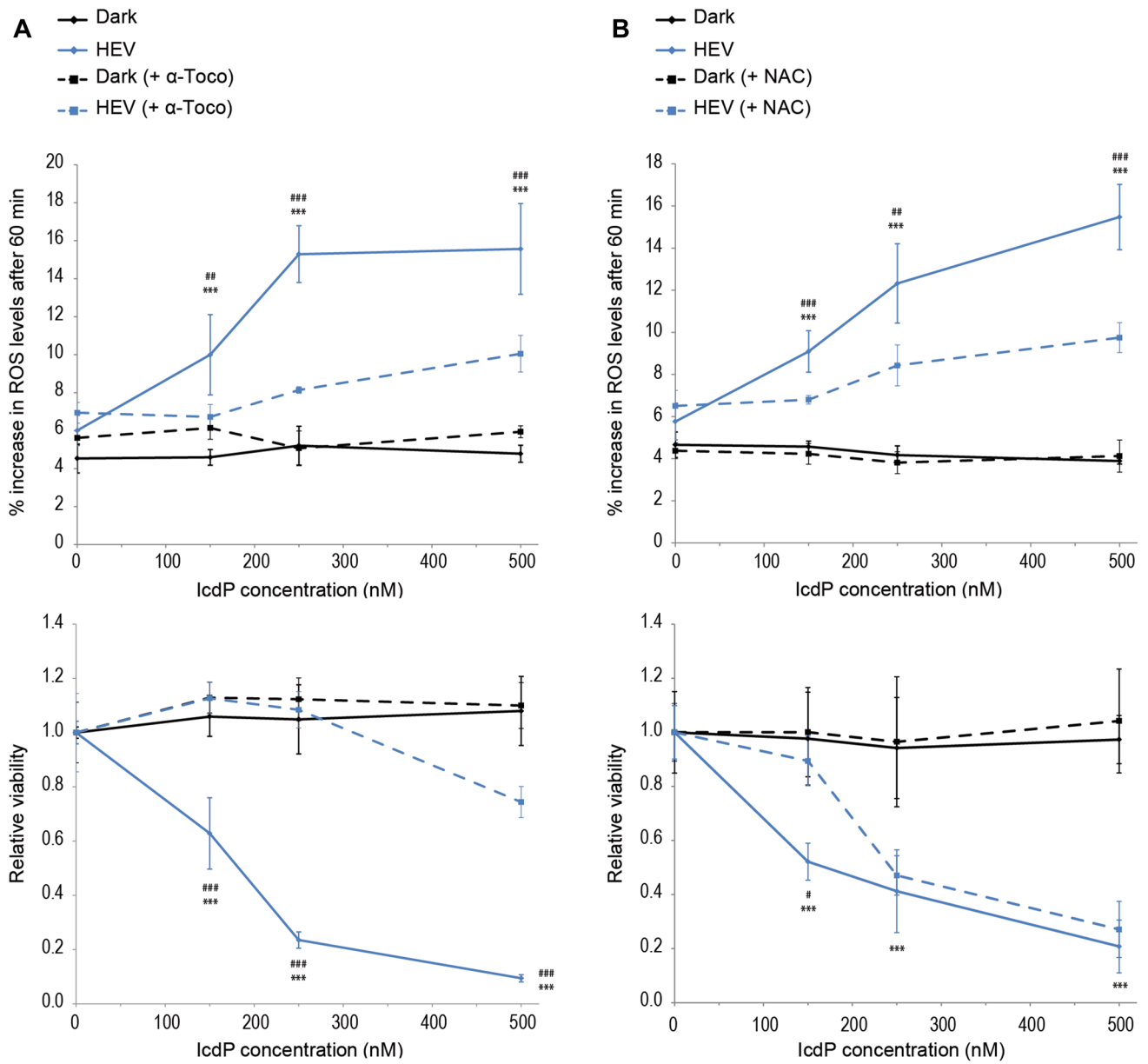

Fig. 6 Antioxidant supplementation effects on ROS accumulation rate and cell viability after co-exposure to IcdP and HEV light. ARPE19 cells were treated with 10 µM α-tocopherol (**a**) or 5 mM *N*-acetylcysteine (**b**) prior co-exposure to IcdP (0, 150, 250 and 500 nM) and 160 J/cm^2 HEV light. ROS accumulation rate in IcdP and/or HEV-exposed cells (with or without antioxidant) was monitored for 60 min after the end of co-exposure using the CM-H_2DCFDA probe (upper panels) and cell viability was measured 24 h post-exposure using the MTS assay (lower panels). Error bars are sd from 4 independent experiments. (*) are for differences between HEV-exposed conditions versus unirradiated controls and ($^{\#}$) are for differences between HEV-exposed conditions versus HEV(+antioxidant)-exposed conditions. *; $^{\#}p < 0.05$, **; $^{\#\#}p < 0.01$ and ***; $^{\#\#\#}p < 0.001$ [one-way analysis of variance (ANOVA) with Tukey HSD procedure as post hoc test]. (Color figure online)

to be concomitant in the cell to exert synergetic toxicity. Our results are even more relevant to real-life exposure since IcdP amount actually reaching the cell in culture may be overestimated. Indeed, it was recently demonstrated that the effective cell-loaded IcdP concentrations may represent only 15% of the initial extracellular concentration (Soeur et al. 2017). In contrast to our study using nanomolar concentrations of PAH, toxicity of PAH alone in RPE cell cultures has been investigated after exposure of cells to extracellular concentrations of 10–100 µM BaP (Patton et al. 2002; Wang et al. 2009) or 200–1000 µM BeP (Sharma et al. 2008). In this study, we observed that acute exposure to IcdP alone, in concentrations of 50–1500 µM induce no loss of RPE cell viability (Fig.

S4). Although the range level of PAH accumulating in the RPE of smokers has never been investigated, it can be assumed from PAH levels in cigarette smoke (Hoffmann et al. 2001; Lodovici et al. 2004; Vu et al. 2015) and from PAH concentrations in circulating blood reported for various populations (Pleil et al. 2010; Soeur et al. 2017), that high-molecular-weight PAH concentrations in RPE should not exceed the nanomolar range. Our experimental PAH exposure conditions are thus closer to what is expected in smokers' RPE in vivo. On that basis, our results indicate that IcdP, upon interaction with HEV light, is a potent candidate initiating the biological mechanisms underlying the association between cigarette smoking and AMD-related RPE degeneration.

An early manifestation of the toxic and metabolic effects caused by IcdP and HEV light synergy is the irreversible collapse of mitochondrial network (Fig. 3). RPE functions require a high metabolic activity. As a result, they must rely on a dynamic and structured network of abundant mitochondria. Feher et al. (2006) previously reported that accelerated age-related decrease of mitochondrial density and deterioration of mitochondrial membranes cristae are observed in AMD-affected RPE (Feher et al. 2006). Since intact mitochondrial membranes are required for the dynamical layout of their network, the extensive disorganization of RPE cells mitochondrial network induced by IcdP and HEV light co-exposure might reflect functional or structural defects of mitochondrial membranes. Along with mitochondrial network collapse, an important oxidative stress is induced in RPE cells by the toxic synergy between IcdP and HEV light (Fig. 5). RPE cells normally possess robust antioxidant defenses (Handa 2012; Kaya et al. 2012). However, the amount of ROS induced as a result of IcdP and HEV outmatches these defenses as shown by the drastic acceleration of ROS accumulation post-co-exposure.

Consistently with the hypothesis that IcdP and HEV light interaction could be involved in AMD-related RPE degeneration, we show that this interaction leads to RPE cell death by apoptosis (Fig. 4). Since antioxidant treatment helps in rescuing cells from death, our results also suggest a major involvement of the IcdP/HEV-induced oxidative stress in RPE cell death (Fig. 6). Nonetheless, compared to the efficient protection against IcdP/HEV-induced cell death observed when using α-tocopherol, the limited ability of NAC to restore RPE cell viability indicates that the origin and/or location of oxidation are important. NAC, a precursor of L-cysteine and reduced glutathione, is a water-soluble scavenger of ROS (Zafarullah et al. 2003). It is thus expected to mainly associate with the aqueous compartments of the cell. In contrast, α-tocopherol is a lipophilic antioxidant which concentrates into lipid storage organelles and cell membranes (Kontush et al. 1996; Urano et al. 1990). Lipophilic high-molecular-weight PAH, such as IcdP, were found to preferentially accumulate in the endoplasmic reticulum, in lysosomes, in cytoplasmic lipid droplets or in membranes including plasma, nuclear and mitochondrial membranes (Ali et al. 2015). Given that α-tocopherol presence in cell hydrophobic spaces seems to offset the consequences of IcdP/HEV-induced oxidation and to prevent the events leading to RPE cells decreased survival (Fig. 6), these sites might be the primary sites of oxidation following a co-exposure to IcdP and HEV light. Hence, as noted earlier for mitochondrial membranes, they may also be specific targets of IcdP and HEV synergy.

In conclusion, IcdP and HEV light synergy rapidly translates into disruption of mitochondrial network and ROS enhanced accumulation, followed by reduction in cell size, nuclear condensation and apoptosis. None of these key features of AMD were observed after exposure to BaP, alone or in combination with HEV light, strengthening the hypothesis that HEV light absorption by IcdP is required for the adverse effects. The current state of understanding of AMD complexity strongly suggests combinatorial mechanisms involving multiple risk factors leading to its onset and progression. In line with this, Fritsche et al. proposed a multi-hit threshold model to explain the onset of AMD only in the late stage of life, even in individuals with inherent genetic susceptibility (Fritsche et al. 2014). They suggest that damage accumulation rate is modified by a set of genetic, age-associated and environmental factors unique to each individual. From this perspective, combination of IcdP and HEV light could synergistically accelerate the acquisition of the threshold level among smokers.

Simultaneous exposure of RPE cells to PAH and HEV light seems inevitable among smokers and our findings highlight the interplay between both environmental risk factors of AMD. We found no cytotoxicity for RPE cells associated with acute exposure to up to 1500 µM of IcdP alone (fig. S4). This strongly suggests that HEV light potentiate, by at least 3000 times, the toxicity of IcdP on RPE cells. In light of our results, investigating the biological processes activated by IcdP and HEV light synergy may provide guidance to a fundamental understanding of AMD pathogenesis. Indeed, through the synergy between them, co-exposure to small amounts of IcdP and HEV light is expected to impair RPE function. Understanding at which level the synergistic mechanisms take place could help uncover critical pathways or apoptotic trigger involved in AMD onset or progression.

Acknowledgements The authors are grateful to the Institut National d'Optique (INO) (Québec, Canada) for technical support. This work was supported by a Grant from the Canadian Institutes of Health Research (CIHR, MOP-133719) to P.J.R. P.J.R. is a research scholar from the Fonds de Recherche du Québec – Santé (FRQ-S).

Author contributions CZ: experiment conception and design, data collection, analysis and interpretation of data, manuscript writing,

and critical revision. PJR: experiment conception and design, critical revision.

Compliance with ethical standards

Conflict of interest The authors declare that they have no conflict of interest.

References

Ali R, Trump S, Lehmann I, Hanke T (2015) Live cell imaging of the intracellular compartmentalization of the contaminate benzo[a]pyrene. J Biophoton 8:361–371. https://doi.org/10.1002/jbio.201300170

Ambati J, Fowler BJ (2012) Mechanisms of age-related macular degeneration. Neuron 75:26–39. https://doi.org/10.1016/j.neuron.2012.06.018

Andriessen EM, Wilson AM, Mawambo G, Dejda A, Miloudi K, Sennlaub F, Sapieha P (2016) Gut microbiota influences pathological angiogenesis in obesity-driven choroidal neovascularization. EMBO Mol Med 8:1366–1379. https://doi.org/10.15252/emmm.201606531

Bertram KM, Baglole CJ, Phipps RP, Libby RT (2009) Molecular regulation of cigarette smoke induced-oxidative stress in human retinal pigment epithelial cells: implications for age-related macular degeneration. Am J Physiol Cell Physiol 297:C1200–C1210. https://doi.org/10.1152/ajpcell.00126.2009

Boettner EA, Wolter JR (1962) Transmission of the ocular media Invest. Ophthalmol Vis Sci 1:776–783

Botta C, Di Giorgio C, Sabatier AS, De Meo M (2009) Effects of UVA and visible light on the photogenotoxicity of benzo[a]pyrene and pyrene. Environ Toxicol 24:492–505. https://doi.org/10.1002/tox.20455

Bourne RR et al (2013) Causes of vision loss worldwide, 1990–2010: a systematic analysis. Lancet Glob Health 1:e339–e349. https://doi.org/10.1016/S2214-109X(13)70113-X

Burke KE, Wei H (2009) Synergistic damage by UVA radiation and pollutants. Toxicol Ind Health 25:219–224. https://doi.org/10.1177/0748233709106067

Chakravarthy U et al (2010) Clinical risk factors for age-related macular degeneration: a systematic review and meta-analysis. BMC Ophthalmol 10:31. https://doi.org/10.1186/1471-2415-10-31

Chiras D, Kitsos G, Petersen MB, Skalidakis I, Kroupis C (2015) Oxidative stress in dry age-related macular degeneration and exfoliation syndrome. Crit Rev Clin Lab Sci 52:12–27 https://doi.org/10.3109/10408363.2014.968703

Dabestani R, Ivanov IN (1999) A compilation of physical, spectroscopic and photophysical properties of polycyclic aromatic hydrocarbons. Photochem Photobiol 70:10–34

Ding YS, Trommel JS, Yan XJ, Ashley D, Watson CH (2005) Determination of 14 polycyclic aromatic hydrocarbons in mainstream smoke from domestic cigarettes. Environ Sci Technol 39:471–478

Ding YS et al (2006) Determination of 14 polycyclic aromatic hydrocarbons in mainstream smoke from U.S. brand and non-US brand cigarettes. Environ Sci Technol 40:1133–1138

Dunaief JL, Dentchev T, Ying GS, Milam AH (2002) The role of apoptosis in age-related macular degeneration. Arch Ophthalmol 120:1435–1442

Ebrahimi KB, Cano M, Rhee J, Datta S, Wang L, Handa JT (2018) Oxidative stress induces an interactive decline in Wnt and Nrf2 signaling in degenerating retinal pigment epithelium. Antioxid Redox Signal. https://doi.org/10.1089/ars.2017.7084

Espinosa-Heidmann DG, Suner IJ, Catanuto P, Hernandez EP, Marin-Castano ME, Cousins SW (2006) Cigarette smoke-related oxidants and the development of sub-RPE deposits in an experimental animal model of dry. AMD Invest Ophthalmol Vis Sci 47:729–737. https://doi.org/10.1167/iovs.05-0719

Feher J, Kovacs I, Artico M, Cavallotti C, Papale A, Balacco Gabrieli C (2006) Mitochondrial alterations of retinal pigment epithelium in age-related macular degeneration. Neurobiol Aging 27:983–993. https://doi.org/10.1016/j.neurobiolaging.2005.05.012

Fritsche LG, Fariss RN, Stambolian D, Abecasis GR, Curcio CA, Swaroop A (2014) Age-related macular degeneration: genetics and biology coming together. Annu Rev Genom Hum Genet 15:151–171. https://doi.org/10.1146/annurev-genom-090413-025610

Fujihara M, Nagai N, Sussan TE, Biswal S, Handa JT (2008) Chronic cigarette smoke causes oxidative damage and apoptosis to retinal pigmented epithelial cells in mice. PLoS One 3:e3119. https://doi.org/10.1371/journal.pone.0003119

Hafezi F, Marti A, Munz K, Reme CE (1997) Light-induced apoptosis: differential timing in the retina and pigment epithelium. Exp Eye Res 64:963–970. https://doi.org/10.1006/exer.1997.0288

Handa JT (2012) How does the macula protect itself from oxidative stress? Mol Aspects Med 33:418–435. https://doi.org/10.1016/j.mam.2012.03.006

Hoffmann D, Hoffmann I, El-Bayoumy K (2001) The less harmful cigarette: A controversial Issue. A Tribute to Ernst L. Wynder. Chem Res Toxicol 14:767–790

Hollyfield JG et al (2008) Oxidative damage-induced inflammation initiates age-related macular degeneration. Nat Med 14:194–198. https://doi.org/10.1038/nm1709

Karbowski M, Youle RJ (2003) Dynamics of mitochondrial morphology in healthy cells and during apoptosis. Cell Death Differ 10:870–880. https://doi.org/10.1038/sj.cdd.4401260

Kaya S et al (2012) Comparison of macular pigment in patients with age-related macular degeneration and healthy control subjects—a study using spectral fundus reflectance. Acta Ophthalmol 90:e399–e403. https://doi.org/10.1111/j.1755-3768.2012.02423.x

King A, Gottlieb E, Brooks DG, Murphy MP, Dunaief JL (2004) Mitochondria-derived reactive oxygen species mediate blue light-induced death of retinal pigment epithelial cells. Photochem Photobiol 79:470–475

Kontush A, Finckh B, Karten B, Kohlschutter A, Beisiegel U (1996) Antioxidant and prooxidant activity of alpha-tocopherol in human plasma and low density lipoprotein. J Lipid Res 37:1436–1448

Lambert NG et al (2016) Risk factors and biomarkers of age-related macular degeneration Progress. Progress Retinal Eye Res 54:64–102. https://doi.org/10.1016/j.preteyeres.2016.04.003

Lerman S (1980) Radiant energy and the eye. Macmillan, New York

Lim LS, Mitchell P, Seddon JM, Holz FG, Wong TY (2012) Age-related macular degeneration. Lancet 379:1728–1738. https://doi.org/10.1016/S0140-6736(12)60282-7

Lodovici M, Akpan V, Evangelisti C, Dolara P (2004) Sidestream tobacco smoke as the main predictor of exposure to polycyclic aromatic hydrocarbons. J Appl Toxicol 24:277–281. https://doi.org/10.1002/jat.992

Marrot L (2017) Pollution and sun exposure: a deleterious synergy. Mechanisms and opportunities for skin protection. Curr Med Chem. https://doi.org/10.2174/0929867324666170918123907

Mauthe RJ, Cook VM, Coffing SL, Baird WM (1995) Exposure of mammalian cell cultures to benzo[a]pyrene and light results in oxidative DNA damage as measured by 8-hydroxydeoxyguanosine formation. Carcinogenesis 16:133–137

Patton WP, Routledge MN, Jones GD, Lewis SE, Archer DB, Davies RJ, Chakravarthy U (2002) Retinal pigment epithelial cell DNA is damaged by exposure to benzo[a]pyrene, a constituent of cigarette smoke. Exp Eye Res 74:513–522. https://doi.org/10.1006/exer.2001.1160

Pleil JD, Stiegel MA, Sobus JR, Tabucchi S, Ghio AJ, Madden MC (2010) Cumulative exposure assessment for trace-level polycyclic aromatic hydrocarbons (PAHs) using human blood and plasma analysis. J Chromatogr B Anal Technol Biomed Life Sci 878:1753–1760. https://doi.org/10.1016/j.jchromb.2010.04.035

Poot M et al (1996) Analysis of mitochondrial morphology and function with novel fixable fluorescent stains. J Histochem Cytochem 44:1363–1372

Putting BJ, Van Best JA, Vrensen GF, Oosterhuis JA (1994) Blue-light-induced dysfunction of the blood-retinal barrier at the pigment epithelium in albino versus pigmented rabbits. Exp Eye Res 58:31–40. https://doi.org/10.1006/exer.1994.1192

Rabin DM, Rabin RL, Blenkinsop TA, Temple S, Stern JH (2013) Chronic oxidative stress upregulates Drusen-related protein expression in adult human RPE stem cell-derived RPE cells: a novel culture model for dry. AMD Aging 5:51–66

Rivera-Figueroa AM, Ramazan KA, Finleyson-Pitts BJ (2004) Fluorescence, absorption and excitation spectra of polycyclic aromatic hydrocarbons as a tool for quantitative analysis. J Chem Educ 81:242–245

Roberto A, Larsson BS, Tjalve H (1996) Uptake of 7,12-dimethylbenz(a)anthracene and benzo(a)pyrene in melanin-containing tissues. Pharmacol Toxicol 79:92–99

Rowan S et al (2017) Involvement of a gut-retina axis in protection against dietary glycemia-induced age-related macular degeneration. Proc Natl Acad Sci USA 114:E4472–E4481. https://doi.org/10.1073/pnas.1702302114

Schirmer K, Chan AG, Greenberg BM, Dixon DG, Bols NC (1998) Ability of 16 priority PAHs to be photocytotoxic to a cell line from the rainbow trout gill. Toxicology 127:143–155

Schmidl D, Garhofer G, Schmetterer L (2015) Nutritional supplements in age-related macular degeneration. Acta Ophthalmol 93:105–121. https://doi.org/10.1111/aos.12650

Sharma A, Neekhra A, Gramajo AL, Patil J, Chwa M, Kuppermann BD, Kenney MC (2008) Effects of Benzo(e)Pyrene, a toxic component of cigarette smoke, on human retinal pigment epithelial cells in vitro. Invest Ophthalmol Vis Sci 49:5111–5117. https://doi.org/10.1167/iovs.08-2060

Soeur J et al (2017) Photo-pollution stress in skin: Traces of pollutants (PAH and particulate matter) impair redox homeostasis in keratinocytes exposed to UVA1. J Dermatol Sci 86:162–169. https://doi.org/10.1016/j.jdermsci.2017.01.007

Sparrow JR, Nakanishi K, Parish CA (2000) The lipofuscin fluorophore A2E mediates blue light-induced damage to retinal pigmented epithelial cells. Invest Ophthalmol Vis Sci 41:1981–1989

Sui GY et al (2013) Is sunlight exposure a risk factor for age-related macular degeneration? A systematic review and meta-analysis. Br J Ophthalmol 97:389–394. https://doi.org/10.1136/bjophthalmol-2012-302281

Thornton J, Edwards R, Mitchell P, Harrison RA, Buchan I, Kelly SP (2005) Smoking and age-related macular degeneration: a review of association. Eye (Lond) 19:935–944. https://doi.org/10.1038/sj.eye.6701978

Urano S, Kitahara M, Kato Y, Hasegawa Y, Matsuo M (1990) Membrane stabilizing effect of vitamin E: existence of a hydrogen bond between alpha-tocopherol and phospholipids in bilayer liposomes. J Nutr Sci Vitaminol (Tokyo) 36:513–519

Vu AT, Taylor KM, Holman MR, Ding YS, Hearn B, Watson CH (2015) Polycyclic Aromatic Hydrocarbons in the Mainstream Smoke of Popular US cigarettes. Chem Res Toxicol 28:1616–1626. https://doi.org/10.1021/acs.chemrestox.5b00190

Wang H, Joseph JA (1999) Quantifying cellular oxidative stress by dichlorofluorescein assay using microplate reader. Free Radic Biol Med 27:612–616

Wang S, Sheng Y, Feng M, Leszczynski J, Wang L, Tachikawa H, Yu H (2007) Light-induced cytotoxicity of 16 polycyclic aromatic hydrocarbons on the US EPA priority pollutant list in human skin HaCaT keratinocytes: relationship between phototoxicity and excited state properties. Environ Toxicol 22:318–327. https://doi.org/10.1002/tox.20241

Wang AL, Lukas TJ, Yuan M, Du N, Handa JT, Neufeld AH (2009) Changes in retinal pigment epithelium related to cigarette smoke: possible relevance to smoking as a risk factor for age-related macular degeneration. PLoS One 4:e5304. https://doi.org/10.1371/journal.pone.0005304

Wielgus AR, Collier RJ, Martin E, Lih FB, Tomer KB, Chignell CF, Roberts JE (2010) Blue light induced A2E oxidation in rat eyes–experimental animal model of dry AMD. Photochem Photobiol Sci 9:1505–1512. https://doi.org/10.1039/c0pp00133c

Wihlmark U, Wrigstad A, Roberg K, Nilsson SE, Brunk UT (1997) Lipofuscin accumulation in cultured retinal pigment epithelial cells causes enhanced sensitivity to blue light irradiatio. Free Radic Biol Med 22:1229–1234

Wong WL, Su X, Li X, Cheung CM, Klein R, Cheng CY, Wong TY (2014) Global prevalence of age-related macular degeneration and disease burden projection for 2020 and 2040: a systematic review and meta-analysis. Lancet Glob Health 2:e106–e116. https://doi.org/10.1016/S2214-109X(13)70145-1

Young RW (1987) Pathophysiology of age-related macular degeneration. Surv Ophthalmol 31:291–306

Zafarullah M, Li WQ, Sylvester J, Ahmad M (2003) Molecular mechanisms of *N*-acetylcysteine actions. Cell Mol Life Sci 60:6–20